JOURNAL OF MATERIALS SCIENCE: MATERIALS IN MEDICINE 6 (1995) 85–89

Structural analyses of carbonate-containing apatite samples related to mineralized tissues

F. J. G. CUISINIER, P. STEUER, J.-C. VOEGEL
INSERM, CJF 92-04, Centre de Recherches Odontologiques 1, Place de l'Hôpital 67000 Strasbourg, France

F. APFELBAUM, I. MAYER
Department of Inorganic and Analytical Chemistry, Hebrew University, Jerusalem 91904, Israel

Crystallographic and structural aspects of two carbonate-containing (one with and another without Zn ions) and a pure hydroxyapatite sample were investigated by high resolution electron microscopy. For five different zone axes and for the three samples a good correspondence was always found between simulated lattice images and observed micrographies. Numerous structural defects were detected in the carbonate-containing apatites, whereas none were found in the similarly prepared pure hydroxyapatite. The incorporation of Zn ions in the crystal lattice of the carbonate-containing apatite reduces the number of defects.

1. Introduction

Calcium phosphates forming inorganic phases of mammal calcified tissues are structurally described by hydroxyapatite (HA) [1]. X-ray diffraction and infrared spectroscopical studies showed that the mineralized calcified tissues could be related to non-stoichiometric carbonate-containing hydroxyapatites [2, 3]. Non-stoichiometry is principally due to ionic losses like calcium deficiencies and/or to ionic substitutions. The most abundant foreign ions are the carbonate ions which either replace OH^- (type A carbonato-apatite) or PO_4^{3-} groups (type B carbonato-apatite) [4, 5]. Ionic losses and substitutions, occurring simultaneously in biological crystals, induce complex structures at the unit-cell level [6, 7]. Synthetic carbonated apatites (c.HAS) are classically used as structural models for the study of the growth and dissolution processes of biological crystals [8, 9]. However, the atomic structure of c.HAS is not completely known because neither pure type A carbonated-apatite nor pure type B carbonated-apatite can yet be synthetized.

Synthetic apatites are currently used for bone restoration and for metallic implant coating in orthopaedics and dentistry. However, in these clinical fields carbonated apatites are only seldom employed. Carbonated apatites possess properties which at first sight could give them interesting clinical potentialities. Among these properties one may in particular notice that:

(a) the presence of carbonate ions within the apatite lattice induces structural disorders as observed for gallium containing carbonate apatites [10] and that the crystallographic defects may subsequently favour biological apatite nucleation;
(b) the presence of carbonate ions increases the solubility product of the samples and for the same pH value, more calcium and phosphate ions are available for the further calcification, or biological mineralization;
(c) as a side effect, the increased solubility of the carbonated apatite may also favour the formation of stronger metal–biological apatite bonds.

Synthetic hydroxyapatite, carbonated apatite and zinc-containing carbonated apatites were studied by high resolution transmission electron microscopy (HRTEM). HRTEM is a powerful tool for the study of crystallized materials with a Scherzer resolution close to 0.15 nm. Unfortunately HRTEM is not so well adapted for the study of non-stoichiometric materials because of the small sizes of the analysed areas and because of the difficulty in detecting chemical variations (except for weak phase objects) [11]. Used for the analyses of calcified tissues, HRTEM allows a precise description of biological crystals with a resolution close to 0.2 nm [12, 13], as well as the characterization of structural defects [13]. The aim of this study was to investigate carefully the structure and morphology of these synthetic apatites and to specify the structural modifications induced by the presence of foreign ions (carbonate and zinc) in the crystal lattice. Particular attention has been paid to the nature and density of structural defects.

2. Materials and methods

2.1. Sample preparation and characterization

Apatite samples were prepared by a precipitation method, precisely described elsewhere [14]. Briefly, the synthesis was performed by the dropwise addition of a phosphate solution (Na_2HPO_4) over 2 h to a stirred Ca solution in the form of $Ca(NO_3)_2$ at 87 °C.

0957–4530 © *1995 Chapman & Hall*

Carbonate was added as $NaHCO_3$ and zinc from a $Zn(NO_3)_2$ solution. After a 2-h reaction, the system was refluxed under boiling for a further 2h. pH was controlled during the synthesis by a pH-stat unit. The precipitate was washed and dried overnight at 120 °C.

The zinc content was determined by the atomic emission spectroscopy method and Fourier transform infrared (FTIR) absorption spectra were obtained with the KBr pellet technique using a Bruker IFS 113v interferometer. Carbonate content was estimated from the i.r. spectra using the extinction ratio at 1415 cm^{-1} (for carbonate) and 575 cm^{-1} (for phosphate) bands [15]. The samples were analysed by X-ray diffraction (XRD) with a Philips automatic powder diffractometer using monochromatized CuK_α radiation.

2.2. HRTEM

Synthetic crystals were suspended in distilled water equilibrated with the same apatite sample. After brief sonication, a drop of the suspension was put on 1000 mesh copper grids covered with carbon-coated Formvar film. All samples were observed without further preparation in a Philips EM 430ST HRTEM equipped with a TV camera (Lhesa, France) and with a low dose unit (Philips, Netherlands). A double tilt specimen holder was used in order to orient crystals along given zone-axes. The parameters of the microscope were an accelerating voltage of 300 kV, a spherical aberration coefficient of 1.1 mm, a beam divergence half-angle of 0.6 mrad. The Scherzer resolution is 0.19 nm. The micrographs were analysed on a laser bench (Micro-Contrôle, France). Zone axis symmetries were defined from optical diffraction diagrams.

2.3. Computer image analysis

High resolution electron images were simulated by means of the EMS program [16] operated on a Silicon Graphics workstation (Mountain View, CA, USA). Simulated images were obtained by the multi-slice method [17] using the atomic positions of hydroxyapatite (HA) [18]. Hydroxyapatite ($Ca_{10}(PO_4)_6(OH)_2$) possesses a hexagonal structure with space group $P6_3/m$. Carbonate replaces either OH^- (A type) or PO_4^{3-} groups (B type) and zinc either replaces calcium in the apatite lattice or is adsorbed on the crystal surface.

3. Results

Three types of apatite samples have been investigated in the present study, namely pure hydroxyapatite (BSO), carbonated apatite (BO1) and Zn-containing carbonate apatite (C23). The analytical composition of these samples is summarized in Table I. The two selected carbonate-containing apatites had carbonate contents close to the one of bone crystals [19]. XRD powder patterns showed that the samples were of single phase and possessed the hexagonal structure of the apatite. The lattice parameters of the hexagonal cell of the three apatites studied were calculated from their powder XRD data and are listed in Table II. These values show the usual effect that carbonate ions have on the lattice parameters of apatites, namely that the carbonate-containing BO1 sample has lower a and higher c values than BSO has. It can also be seen that, in the case of the C23 sample with 4.5% Zn content, an additional decrease of the lattice constants occurs. This is apparently caused by the incorporation of the relatively small Zn^{2+} ions in the apatite lattice as was observed in many Zn-containing carbonate apatites [20]. FTIR spectra of these samples showed the characteristic OH^-, water, carbonate and phosphate vibration bands of the apatites.

The general crystal shapes could be directly observed on the micrographs. Hydroxyapatite crystals (BSO) showed the most regular shape (Fig. 1a), where-

TABLE I Composition of hydroxyapatite sample (BSO), carbonate apatite sample (BO1) and Zn-containing carbonate apatite C23

	BSO	BO1	C23
pH of preparation	9.0	9.0	9.0
Carbonate content (%)	0	6.3	4.5
Zinc content (μg/g)	0	0	45000

TABLE II Lattice constants of studied apatites

Sample	Lattice constants	
	a (nm)	c (nm)
BSO	0.9428	0.6884
BO1	0.9402	0.6917
C23	0.9391	0.6890

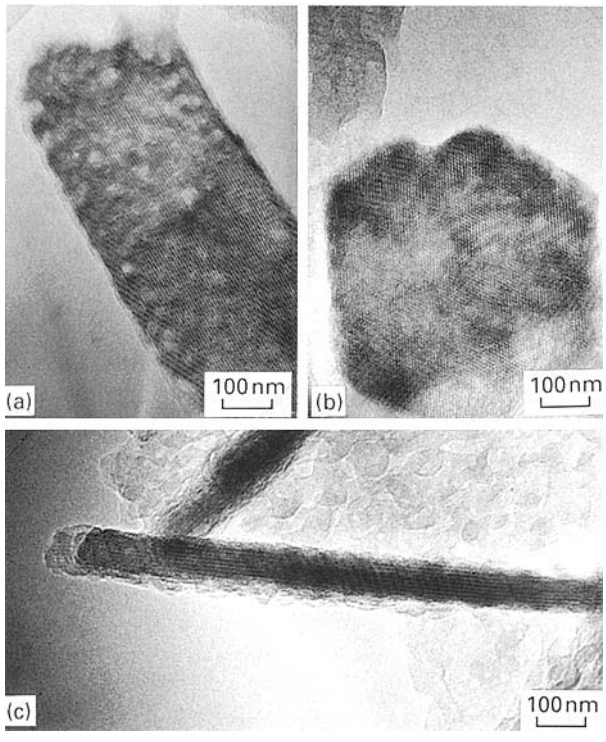

Figure 1 Low magnification micrograph of (a) a pure hydroxyapatite crystal (BSO); (b) a carbonate apatite crystal (BO1); (c) Zn-containing carbonate apatite crystals (C23).

as carbonated apatite crystals (BO1) had a more irregular shape (Fig. 1b). Zn-containing carbonate apatite crystals possess a platelet-like habit demonstrated by their systematic ribbon-like appearance (Fig. 1c) when laterally observed.

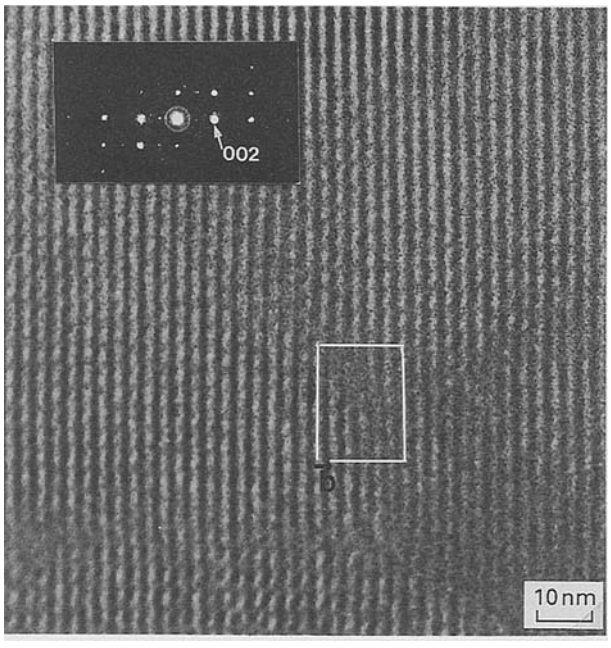

Figure 2 Edge dislocation in a Zn-containing apatite crystal with a Burgers vector **b** = [002]; insert: optical diffractogram ⟨210⟩ zone axis.

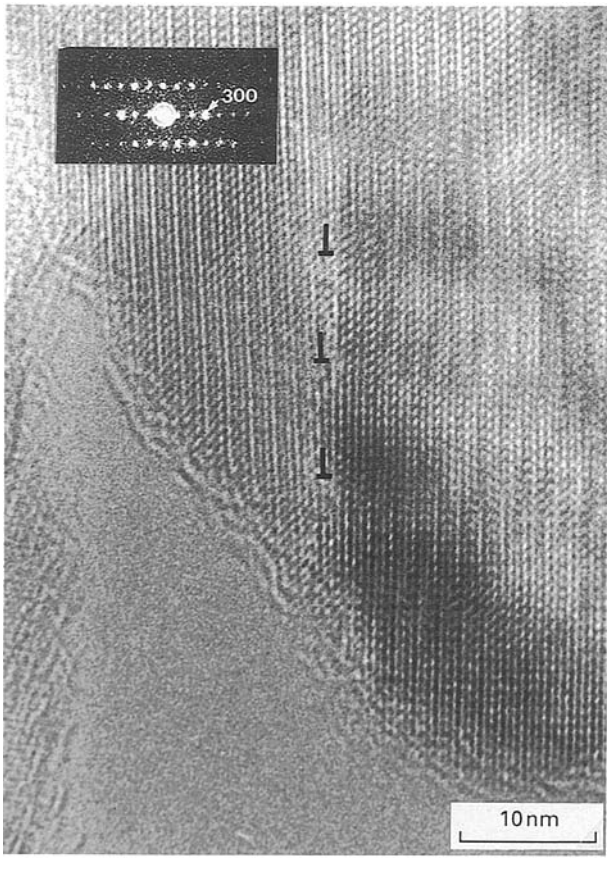

Figure 3 Tilt boundary in a Zn-containing apatite crystal, angle θ = 3.8°, distance D = 4.1 nm between edge dislocations, ⊥: edge dislocation with Burgers vector **b** = [300]; insert: optical diffractogram ⟨210⟩ zone axis.

Dislocations were characterized with the aid of Burgers circuits in order to define Burgers vectors. A Burgers circuit was drawn for a dislocation found in a Zn-containing apatite crystal observed along the ⟨210⟩ zone axis (Fig. 2). The value of the Burgers vector is **b** = [002]. The dislocation is perpendicular to the Burgers vector and has an edge character. It is an imperfect dislocation with Burgers vector perpendicular to the basal [100] plane of HA and possesses a σS character as classicaly described for hexagonal close packed lattices [21]. The length of the Burgers vector is 0.344 nm. A typical low angle boundary was

TABLE III Number of crystals showing structural defects (dislocations and grain boundaries)

	BSO	BO1	C23
Crystals showing structural defects (%)	0	36	20

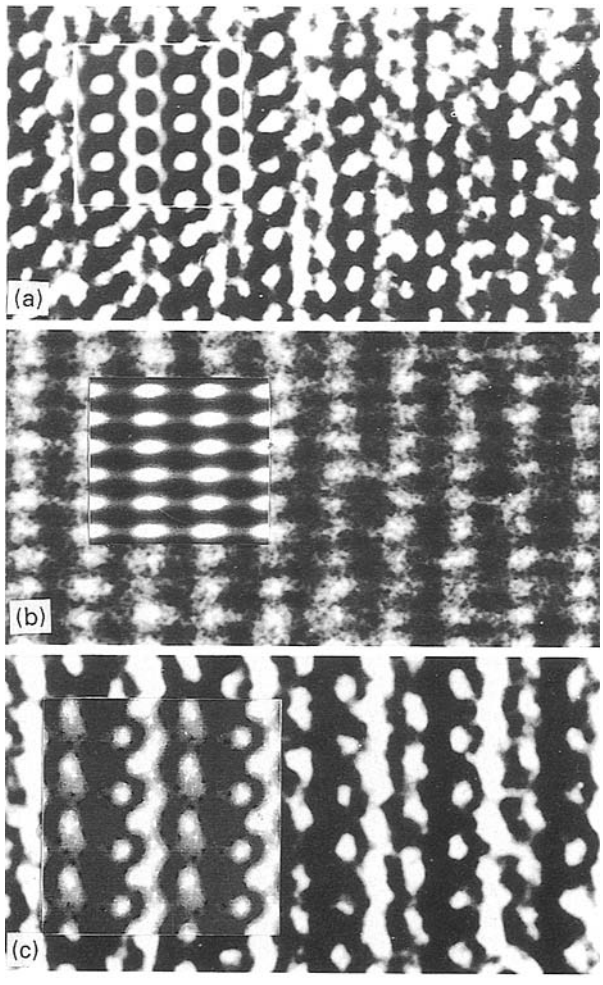

Figure 4 Synthetic apatite crystals observed along ⟨102⟩ zone axis: (a) hydroxyapatite (BSO); insert: computer-calculated image of 2 × 2 unit cells of HA, objective lens defocus value 56 nm, specimen thickness 23.4 nm, aperture shift (030), beam tilt (030); (b) carbonate apatite (BO1); insert: computer-calculated image of 3 × 3 unit cells of HA, objective lens defocus value 84 nm, specimen thickness 6.6 nm; (c) Zn-containing carbonate apatite (C23); insert: computer-calculated image of 2 × 2 unit cells of HA, objective lens defocus value 77 nm, specimen thickness 35 nm, aperture shift (030), beam tilt (030).

also observed in a crystal aligned along the ⟨102⟩ axis (Fig. 3). This boundary is a tilt boundary formed by edge dislocations. (The slit plane of the grain boundary is parallel to $(10\bar{1}0)$ lattices planes.) The boundary is characterized by an angle θ of 3.8° between the two grains and a distance D of 4.11 nm between edge dislocations. For each sample type, three different structural defects were recorded (screw and edge dislocations and grain boundaries) (see Table III). The importance of the carbonate ion incorporation in the induction of structural defects is clearly demonstrated by the total absence of such defects in the BSO sample prepared similarly, but without carbonate ions.

TABLE IV Number of crystals observed along 11 zone axes

Zone axis	Number of crystals (BSO)	Number of crystals (BS1)	Number of crystals (C23)
⟨001⟩	1	3	2
⟨100⟩	3	2	1
⟨111⟩	6	1	3
⟨102⟩	1	1	2
⟨221⟩	1	1	1
⟨210⟩	1		8
⟨310⟩			1
⟨201⟩			1
⟨520⟩		2	1
⟨211⟩		1	
⟨431⟩	1		1

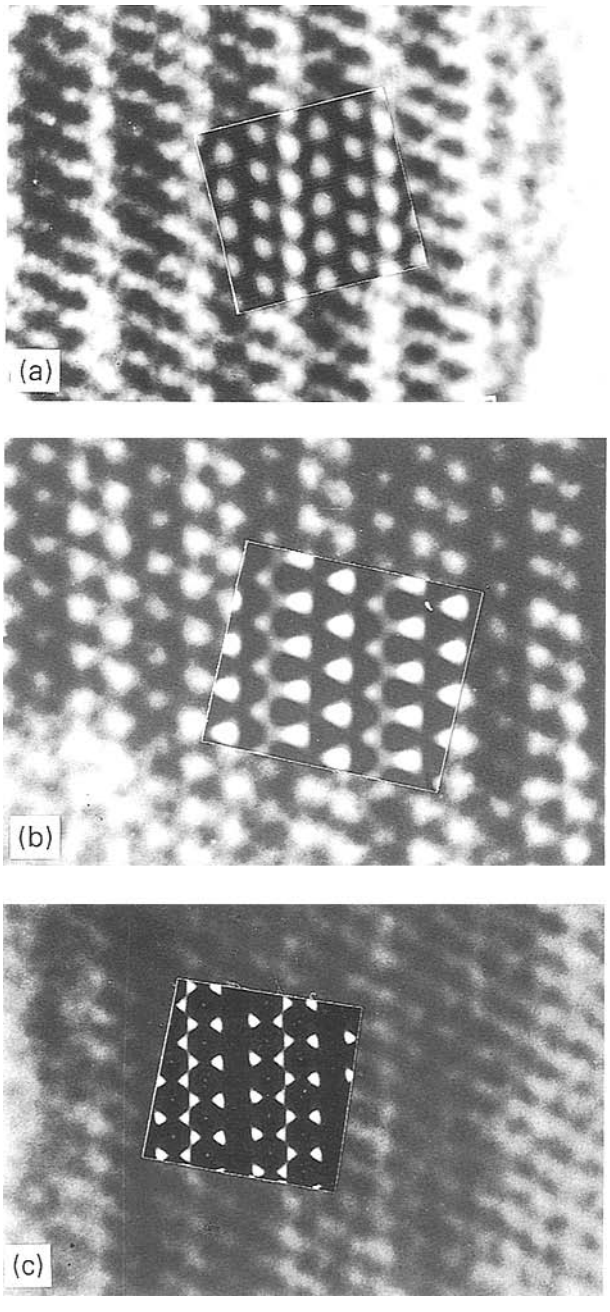

Figure 5 Synthetic apatite crystals observed along ⟨221⟩ zone axis: (a) hydroxyapatite (BSO); insert: computer-calculated image of 2 × 2 unit cells of HA, objective lens defocus value 21 nm, specimen thickness 20 nm, aperture shift $(\bar{2}11)$; (b) carbonate apatite (BO1); insert: computer-calculated image of 2 × 2 unit cells of HA, objective lens defocus value 14 nm, specimen thickness 4 nm, beam tilt $(\bar{1}10)$; (c) Zn-containing carbonate apatite (C23); insert: computer-calculated image of 2 × 2 unit cells of HA, objective lens defocus value 42 nm, specimen thickness 20 nm, aperture shift $(\bar{2}12)$.

The crystals were observed, with a resolution close to 0.2 nm, along 11 different zone axes (Table IV). BSO crystals were most often seen along the ⟨111⟩ zone axis, BO1 crystals along the ⟨001⟩ zone axis and C23 crystals along the ⟨221⟩ zone axis. For the three samples and the five zone axes computer-simulated images of hydroxyapatite were compared to experimental ones. BSO (Fig. 4a), BO1 (Fig. 4b) and C23 (Fig. 4c) crystals observed along ⟨102⟩ all show that observed images were closely related to the HA structure. The same approach was used to investigate HRTEM images along the ⟨221⟩ zone axis. Here again simulated structure could be fairly related to observed images for BSO (Fig. 5a), BO1 (Fig. 5b) and C23 (Fig. 5c). For the three other directions (data not presented) a good correspondence was also found systematically between simulated lattice images and observed crystals.

4. Discussion

The incorporation of foreign (Zn or carbonate) ions in the crystal lattice appeared to modify strongly the habit of pure hydroxyapatite. The shape characteristics were observed on low (Fig. 1), as well as on high (Fig. 2) magnified crystal images. BSO crystals possess a general bulky shape as deduced from the similar plate-like habit found when observed along the ⟨100⟩ and ⟨111⟩ zone axes, but they were also less irregularly shaped than BO1 crystals. We propose a platelet-shape for C23 crystals, since a ribbon-like habit is seen along the ⟨001⟩ and ⟨102⟩, as well as along the ⟨100⟩ zone axes. These platelet crystals also appear to be bent. From these two morphological characteristics C23 crystals seem to be fairly related to biological bone [22] or developing enamel crystals [23]. The specific morphology of each crystal type certainly also explains the preferential observations of certain zone axes (Table III). So, six BSO and eight C23 crystals were, respectively, found along ⟨111⟩ and ⟨210⟩ zone axes.

The study of the carbonate-containing apatite crystals showed also that most of them had structural defects, dislocations and grain boundaries, whereas

the similarly prepared pure hydroxyapatite crystals had no structural defects. The addition of Zn seems also to confirm Zn substitution (at least partly) within the crystal lattice instead of adsorption on the crystal surface. We showed previously that 40 % of the Ga-containing apatite crystals presented structural defects [10]. We can also postulate that a carbonate incorporation of 4.5–6 % (weight percentage) in the crystal lattices increases the number of structural defects. The addition of metallic ions has itself an incidence on these defects, more specifically Ga seems to increase and Zn to decrease the number of crystals showing structural defects. Dissolution results obtained recently [20] for Zn-containing carbonate apatites seem to be in good agreement with the present observations. The mean dissolution rates in the presence of Zn were found to be lower than for no zinc-containing samples: 4.6–5.9 ppm Ca/hour (for the samples with Zn) and 6.4–8.6 ppm Ca/hour (for the samples without Zn).

In conclusion, this HRTEM study allowed the observation of 64 crystals (from three types of apatite samples) along seven different zone axes. Observed images fitted well with simulated HA crystal structures for five different crystallographic axes. Compared to carbonated apatites, Zn substitution leads to a decrease of the number of structural defects, which are totally absent from pure hydroxyapatite.

Acknowledgements

The authors acknowledge the Foundation J. J. Goupil for financial support, and thank also N. Fournier for photographic printing and H. Zins for typing the manuscript.

References

1. W. F. DEJONG, *Red. Trav. Pays-Bas* **45** (1926) 445.
2. D. MACCONNEL, "Apatite" (Springer-Verlag, New York, 1973).
3. W. H. EMERSON and E. E. FISCHER, *Arch. Oral. Biol.* **7** (1962) 671.
4. G. BONEL and G. MONTEL, *Cr. Acad. Sci. Paris* **258** (1964) 923.
5. M. VIGNOLES, G. BONEL, D. HOLCOMB and R. A. YOUNG, *Calcif. Tissue Res.* **43** (1988) 33.
6. D. G. A. NELSON, G. J. WOOD and J. C. BARRY, *Ultramicroscopy* **19** (1986) 253.
7. D. G. A. NELSON, *J. Dent. Res.* **60** (1981) 1621.
8. B. R. HEYWOOD, N. H. C. SPARHS, R. P. SHELLIS, S. WEINER and S. MANN, *Connect. Tiss. Res.* **25** (1990) 1.
9. J. ARENDS and W. L. JONGEBLOED, *J. Dent. Res.* **58B** (1979) 837.
10. F. J. G. CUISINIER, J. C. VOEGEL, F. APFELBAUM and I. MAYER, *J. Crystal Growth* **125** (1992) 1.
11. F. J. G. CUISINIER, R. W. GLAISHER, J. C. VOEGEL, J. HUTCHISON, E. F. BRÈS and R. M. FRANK, *Ultramicroscopy* **36** (1991) 297.
12. D. G. A. NELSON and J. D. MCLEAN, *Tooth enamel V.* Elsevier, Amsterdam, (1984) 47–51.
13. F. J. G. CUISINIER, P. STEUER, R. M. FRANK and J. C. VOEGEL, *J. Biol. Buccale* **18** (1990) 149.
14. J. D. B. FEATHERSTONE, I. MAYER, F. C. M. DRIESSENS, R. M. H. VERBEECK and H. J. M. HEIJLIGERS, *Calcif. Tissue Int.* **35** (1983) 169.
15. J. D. B. FEATHERSTONE, S. PEARSON and R. Z. LEGEROS, *Caries Res.* **18** (1984) 63.
16. P. STADELMANN, *Ultramicroscopy* **21** (1987) 131.
17. J. M. COWLEY, *Acta. Crystallogr.* **12** (1959) 367.
18. M. I. KAY, R. A. YOUNG and A. S. POSNER, *Nature* **204** (1964) 1050.
19. G. MONTEL, G. BONEL, J. C. HEUGHEBAERT, J. C. TROMBE and C. REY, *J. Crystal Growth* **53** (1981) 74.
20. I. MAYER, F. APFELBAUM and J. D. B. FEATHERSTONE, *Archs. Oral. Biol.* (in press).
21. D. HULL, "Introduction to dislocations", 3rd Edn (Pergamon, Oxford, 1984).
22. F. J. G. CUISINIER, E. F. BRÈS, J. HEMMERLÉ, J. C. VOEGEL and R. M. FRANK, *Calcif. Tissue Int.* **40** (1987) 332.
23. F. J. G. CUISINIER, P. STEUER, B. SENGER, J. C. VOEGEL and R. M. FRANK, *ibid.* **51** (1992) 259.
24. I. MAYER, R. GLENA and J. D. B. FEATHERSTONE (unpublished results).

Received 27 October
and accepted 20 December 1993